

# STUDY OF THE PRINCIPLE OF A NOVEL HYBRID DC COMPARATOR

**Li Weibo Ma Weiming Zhao Zhihua Xu Jin Xiao Huan**

National Key Laboratory for Vessel Integrated Power System Technology

Naval Engineering University, Wuhan, 430033, China

E-mail: [hustlwb@hotmail.com](mailto:hustlwb@hotmail.com)

## ABSTRACT

*The traditional controllable saturation reactor (CSR) consists of single toroidal core, DC (direct current) controlled loop (including DC controlled winding and DC biasing source) and AC (alternating current) excitation loop (including excitation winding and AC source). A detection winding and secondary winding are added up to the CSR configuration and form a hybrid DC comparator. Research shows the terminal voltage of the detection winding is asymmetric waveform when the secondary winding of the comparator is open and the CSR core is stimulated both by AC and DC biased sources. Both theory analysis and experiment verify the feasibility of the differential RMS (root-mean-square) between positive and negative half waves of the terminal voltage from the detection winding fitted for the feedback variance to balance DC biasing magnetic potential and form a self-balancing comparator. The zero-flux technique that the primary ampere-turn is equal to the secondary is the function base for the comparator. The operation details of the comparator including the control characteristics both of open-loop and close loop, the satiability judgment criterion, static error property and test range are introduced. The experimental results testify to the truth of the principle of the proposed DC comparator.*

**Key words** Controllable Saturation Reactor, DC Comparator, Sensor.

## 1. INTRODUCTION

The controllable saturation reactor (CSR) is device with magnetic nonlinearity and widely used in such as the power transmission lines, DC comparators, stable sources and so on, see [1]. The configuration of the CSR includes single toroidal core, DC controlled loop composed of DC source and DC winding (also called primary winding,  $W_1$ ) and AC excitation loop made of AC source and excitation winding ( $W_s$ ). The operation principle of the CSR is expressed as follows: the ampere-turn combined by AC and DC can be increased directly if the current through CSR is

increasing; at some point, this causes a decrease in the permeability of the core; with the permeability of the core decreased, the inductance of the winding decreases; a decrease in the inductance causes an increase in power through the load. Changing the permeability of the core controls the reactance of CSR. Varying the flux in one direction through the core when the CSR is stimulated by AC voltage source changes the permeability of the core. Depending on saturation principle they can be divided on DC controllable reactors (DCCR) or AC (alternating current) controllable reactors (ACCR) [2, 3].

*Received Date:* 01.01.2008

*Accepted Date:* 01.07.2008

Conventional DC comparators such as magnetic modulator comparator (MMC) and magnetic amplifier comparator (MAC) are applied widely to measure DC. They adopt two symmetric ferromagnetic cores, four windings (i.e. primary winding  $W_1$ , secondary winding  $W_2$ , excitation winding  $W_S$  and detection winding  $W_M$ ) and peripheral circuits. The measurement goal is accomplished by way of the zero-flux technique that the primary ampere-turns  $I_1W_1$  is equal to the secondary ampere-turns  $I_2W_2$  (i.e.  $I_1W_1=I_2W_2$ ). As a result, they have high accuracy.

And their important difference can be generalized as follows: they have their own methods for acquiring the feedback variance. With concrete analysis, the double frequency signal of the induced voltage of the detection winding is adopted as the feedback variance for MMC when the two cores are excited both by the auxiliary AC voltage source and DC biasing source. The odd harmonic components of the auxiliary AC current source used to excite the two cores for MAC are adopted as the feedback variance. MMC has the characteristics of high sensitivity to the weak current and low drift and MAC has the characteristics of no false-balancing points and high linearity. However, they have such disadvantages that MMC has unsatisfactory output characteristic that zero output points not only at the operating point corresponding to zero ampere-turn but also at the false-balance points. Research indicates the so-called false-balance points affect not only the current ratio, but also the stability and reliability of the comparator. And the usual MAC has too large an electrical inertia to follow the small values of direct current [5-8].

A novel hybrid DC comparator for overcoming the defects of the available two

comparators above is presented in the paper. And it is centered on the configuration of the CSR with some proper modifications, which is a necessary condition for the proposed comparator. The added two windings that are respectively called detection winding  $W_M$  and secondary winding  $W_2$  (also called feedback winding) are wound around the CSR core. And the hybrid comparator is made of four windings like the available DC comparator above (i.e. primary, secondary, detection, and excitation windings), a toroidal core and peripheral circuit that composed of AC excitation source, DC biasing source, the feedback loop, and the display loop. The schematic diagram of the proposed DC comparator is demonstrated in Fig.1.

The winding on the left upper part is called primary winding with  $W_1$ -turns and is connected to a reactor  $L_1$  functioning as a ripple filter and a rheostat  $R_1$  including wire and winding resistance. The winding on the left lower part called excitation winding with  $W_S$ -turns is connected a current-limiting resistor  $R_S$ . The CSR core is stimulated both by AC source ( $u_S$ ) and DC biasing source. The winding on the right lower part is called secondary winding with  $W_2$ -turns and is connected to a current-limiting resistor  $R_2$  and a ripple filter reactor  $L_2$ . The winding on the right upper part is called detection winding with  $W_M$ -turns and is connected to a terminal resistor  $R_M$ . The increment of the controlled biasing current will cause the amount of magnetism in the saturation core to increase and the inductance of the winding in the load circuit to decrease (because the toroidal core is common to four windings). The detection winding can disclosure the alternation of the flux of the core based on the law of electromagnetic induction.

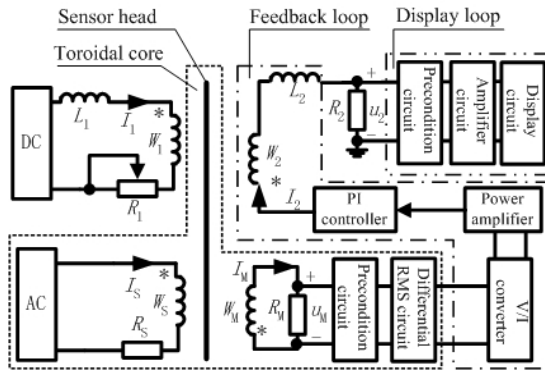


**Fig.1** Schematic diagram of the hybrid DC comparator centered on CSR configuration

The feedback loop includes V/I converter, PI (proportional integral) controller, power amplifier and feedback winding. The feedback loop functions to provide feedback variance for the comparator and track the measured current,  $I_1$ , in real time.

The precondition circuit, amplifier circuit and display circuit form the display loop, whose function is to acquire and deal with secondary current data for calculating and displaying the measured current (also called primary current)  $I_1$ .

## 2. Operation principle of the hybrid dc comparator

### 2.1 Fundamentals of the comparator centered on CSR

Assuming that B-H curves of the CSR is the ideal three-fold line, which means magnetization and permeability curves for a CSR is the ideal operating point. The idea operating point is the place in which a small increase in biasing DC will cause a large increase in output power and a small decrease in biasing DC will cause a large decrease in output power. This point is on the flattest portion of the permeability curve (after its

peak) and called knee of the curve. The knee of the curve is the point of maximum curvature. CSR and magnetic amplifier should be operated on the knee of the magnetization curve. The prerequisite is a good knowledge of the following fundamentals of the proposed comparator.

In the following discussion we assume the primary current  $I_1$  be positive (i.e.  $I_1 > 0$ ) marked in Fig.1. Thus, equations of the electric and magnetic circuits are expressed as

$$u_s = R_s i_s + W_s S \frac{dB}{dt} \quad (1)$$

$$i_s + I_1' = i \quad (2)$$

$$B = f(H) \quad (3)$$

where  $S$  is cross-area of the saturation core.  $i_s$  is AC excitation current passing along the excitation winding.  $B$  and  $H$  are magnetic induction and intensity.  $i$  is called the equivalent excitation current for stimulating magneto-motive force (MMF). Voltage  $u_s$  can be expressed as  $u_s = U_{sm} \sin \omega t$ , where  $U_{sm}$

is the peak value. The angular frequency is expressed as  $\omega = 2\pi f$ , where  $f$  is the frequency of the AC excitation source.  $I_1'$  and  $i$  can be respectively determined by

$$I_1' = W_1 I_1 / W_s \quad (4)$$

$$i = Hl / W_s \quad (5)$$

where  $l$  is the average length of the core.  $I_1$  is called the measured current (also called biasing DC) passing along the DC winding. A premise is given that the magnetic property of the core is in the critical situation between saturation and under-saturation state when the core is stimulated only by AC source. As a

result,  $U_{Sm}$  equals

$$U_{Sm} = U_{Sat} = W_S S \omega B_S = 2\pi f W_S S B_S \quad (6)$$

where  $U_{Sat}$  is peak value of the critical situation of the AC source.  $B_S$  is the saturation magnetic induction. Guessing the initial value of the magnetic state is  $B_S$  when  $\omega t=0$ . During the duration of  $0 \leq \omega t \leq \pi + \beta$ , the magnetic situation of the core is in the saturation state. Assuming that excitation winding is independent of the primary winding, hence,  $i_s$  and  $i$  can be deduced as

$$i_s = u_s / R_S = U_{Sm} \sin \omega t / R_S \quad (7)$$

$$i = U_{Sm} \sin \omega t / R_S + W_1 I_1 / W_S \quad (8)$$

As  $\omega t = \pi + \beta$ ,  $i=0$ , angle  $\beta$  equals

$$\beta = \arcsin[R_S I_1 W_1 / (U_{Sm} W_S)] \quad (9)$$

and angle  $\beta$  is limited as

$$0 \leq \beta \leq \pi / 2 \quad (10)$$

Analysis of the equations (6), (9) and (10) enable us to conclude that the range ability of measured current  $I_1$  can be limited as

$$I_1 \leq W_S U_{Sm} / (R_S W_1) = 2\pi f W_S^2 S B_S / (R_S W_1) \quad (11)$$

Equation (11) indicates that the maximum range ability of current  $I_1$  is dependent on such parameters as  $B_S$ ,  $W_S$ ,  $R_S$ ,  $W_1$ ,  $S$  and  $f$ .

During the duration of  $0 \leq \omega t \leq \pi + \beta$ , the terminal voltage of the detection winding is zero and shown as

$$u_M = 0 \quad (12)$$

During the duration of  $\pi + \beta \leq \omega t \leq 2\pi + \alpha$ , the magnetic property is in the under-saturation state. Thus,  $i=0$ ,  $H=0$ .  $\alpha$  is called saturation angle. AC excitation current equals

$$i_s = -I_1' \quad (13)$$

During the duration of  $\pi + \beta \leq \omega t \leq 2\pi - \beta$ , the magnetic induction  $B$  is decreased from  $B_S$  to minimum  $B_{min}$ . During the duration of  $2\pi - \beta \leq \omega t \leq 2\pi + \alpha$ , the magnetic induction  $B$  is increased from minimum  $B_{min}$  to  $B_S$ . The magnetic induction of the core can be deduced as

$$B = \frac{1}{W_S S} \left( \frac{-1}{U_{Sm} \omega} \cos \omega t + \frac{R_S W_1 I_1}{\omega W_S} \omega t \right) + B_S \quad (14)$$

When  $\omega t = 2\pi$ , the minimum magnetic induction equals

$$B_{min} = \frac{1}{W_S S} \left( \frac{-1}{U_{Sm} \omega} + \frac{2\pi R_S W_1 I_1}{\omega W_S} \right) + B_S \quad (15)$$

During the duration of  $\pi + \beta \leq \omega t \leq 2\pi + \alpha$ , the total maximum increment of the magnetic induction is zero and an important equation can be deduced

$$(\cos \beta + \cos \alpha) = (\pi + \alpha - \beta) \sin \beta \quad (16)$$

It follows that angle  $\alpha$  can be solved by substituting solution of angle  $\beta$  into Eqn. (16). During duration of  $\pi + \beta \leq \omega t \leq 2\pi - \beta$  or  $2\pi - \beta \leq \omega t \leq 2\pi + \alpha$ , the terminal voltage of the detection winding both equals

$$u_M = \frac{W_M}{W_S} \left( U_{Sm} \sin \omega t + \frac{R_S W_1 I_1}{W_S} \right) \quad (17)$$

During the duration of  $2\pi + \alpha < \omega t \leq 3\pi + \beta$ , the magnetic state of the core is in the saturation state (i.e.  $B=B_S$ ), so that the terminal voltage of the detection winding is zero. The analysis details are the same to the duration of  $0 \leq \omega t \leq \pi + \beta$ . When  $\omega t = 3\pi + \beta$ ,  $i=0$ ,  $H=0$ . Then next analysis period is restarted.

Typical waveforms of  $u_S$ ,  $B$ ,  $I_1'$ ,  $i_S$ ,  $i$  and  $u_M$  are respectively demonstrated in Fig.2 (a) ~ (f).

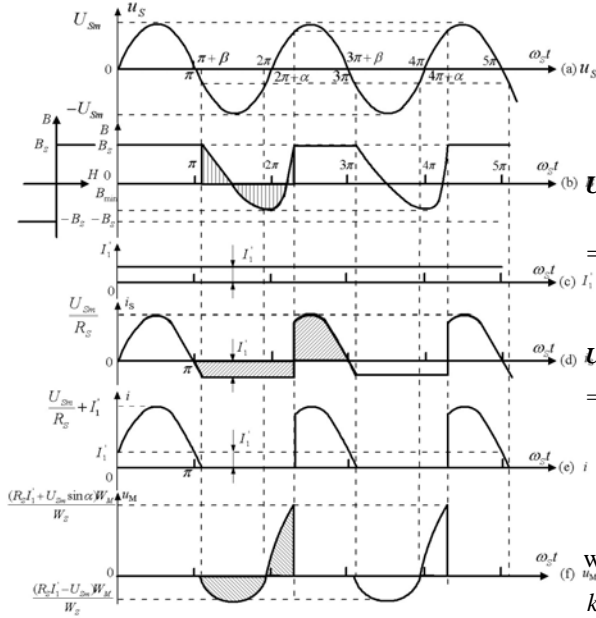


**Fig.2** Typical waveforms  $u_S$ ,  $B$ ,  $I_1'$ ,  $i_S$ ,  $i$  and  $u_M$  ( $I_1 > 0$ )

During duration of  $\pi + \beta < \omega t \leq 3\pi + \beta$ , though the average value of the terminal voltage  $u_M$  is zero, upon analyzing above Eqn. (17), we got the following set of equations of the minimum, maximum, and peak-peak values of the terminal voltage:

$$U_{MN} = \frac{W_M}{W_S} (R_S \frac{W_1 I_1}{W_S} - U_{Sm}) \quad (18)$$

$$U_{MP} = \frac{W_M}{W_S} (R_S \frac{W_1 I_1}{W_S} + U_{Sm} \sin \alpha) \quad (19)$$

$$U_{MPP} = U_{MP} - U_{MN} = U_{Sm} W_M (1 + \sin \alpha) / W_S \quad (20)$$

Hence, RMS values of the positive half-wave, negative half-wave, and full-wave of the voltage ( $u_M$ ) are respectively deduced as

$$U_{MRMSP} = \sqrt{\frac{1}{2\pi} \int_{\pi-\beta}^{2\pi-\alpha} u_M^2 d\omega t} = k_0 \sqrt{(\alpha + \beta)k_1 - k_2(\sin 2\alpha + \sin 2\beta) + k_3(\cos \beta - \cos \alpha)}$$

$$U_{MRMSN} = \sqrt{\frac{1}{2\pi} \int_{\pi-\beta}^{2\pi-\alpha} u_M^2 d\omega t} = k_0 \sqrt{(\pi - 2\beta)k_1 + 2k_2 \sin 2\beta - 2k_3 \cos \beta} \quad (22)$$

$$U_{MRMS} = \sqrt{U_{MRMP}^2 + U_{MRMN}^2} = k_0 \sqrt{(\pi + \alpha - \beta)k_1 + k_2(\sin 2\beta - \sin 2\alpha) - k_3(\cos \beta + \cos \alpha)} \quad (23)$$

where  $k_0 = W_M / (\sqrt{2\pi} W_S)^{-1}$ ,  $k_2 = U_{Sm}^2 / 4$ ,  $k_1 = U_{Sm}^2 / 2 + (R_S I_1 W_1 / W_S)^2$ ,  $k_3 = 2U_{Sm} R_S I_1 W_1 / W_S$ . Hence, the differential RMS value,  $U_{MdiffRMS}$ , equals

$$U_{MdiffRMS} = U_{MRMSP} - U_{MRMSN} \quad (24)$$

From equations (18) ~ (24) it can be concluded that the minimum, maximum, peak-peak, differential RMS values of the terminal voltage ( $u_M$ ) has relation to the DC biasing ampere-turn,  $I_1 W_1$  (or the primary ampere-turn).

When the direction  $I_1$  is negative (i.e.  $I_1 < 0$ ), analysis method for the negative current  $I_1$  are the same to the positive current (i.e.  $I_1 > 0$ ) and more detailed description are omitted.

### 2.2 Close-loop principle of the hybrid DC comparator

The fundamentals of the proposed comparator are the saturation property of the CSR. And the saturation phenomenon of the core might

occur severely when the AC excitation current ( $i_s$ ) and DC biasing current ( $I_1$ ) are too large. The terminal voltage ( $u_M$ ) has some high-frequency components (i.e. 3<sup>rd</sup>, 5<sup>th</sup> order harmonic components, et. al.) due to the saturation property of the core, which is particularly disturbing the waveform of the terminal voltage ( $u_M$ ) and will give severe influences to the computation accuracy of the minimum ( $U_{MN}$ ), maximum ( $U_{MP}$ ), and peak-peak ( $U_{MPP}$ ).

With the differential RMS  $U_{MdiffRMS}$ , things are different. The RMS theory emphasizes the comprehensive impacts induced by all components of the terminal voltage. Thus the differential RMS  $U_{MdiffRMS}$  will give few considerations of the odd harmonic or even harmonic components of the terminal voltage, which can guarantee the high sensitivity of the comparator. One of the greatest advantages of this method is its great simple peripheral circuit in respect that the adoptions of RMS ICs (e.g. AD736/AD737) and an adder circuit can easily accomplish the function of the method and acquire the differential RMS signal.

Consequently, by referring to the simplified schematic diagram of Fig.1, the close-loop operation principle of the proposed comparator is described as follows:

Firstly, the terminal voltage ( $u_M$ ) is acquired and preconditioned. Secondly, resorting to the RMS ICs (e.g. AD736/AD737) and an adder circuit, the differential RMS voltage ( $U_{MdiffRMS}$ ) is obtained and turned into the current by the V/I converter circuit. Thirdly, the current is amplified by the power amplifier and regulated by the PI controller. And the amplified current is specially called the secondary current  $I_2$ . Fourthly, the

secondary current  $I_2$  flows into the secondary winding and produces a reversed magnetic potential (i.e.  $I_2W_2$ , also called secondary number-turn) with regard to the primary one for balancing the DC biasing magnetic potential in the core. When the total DC biasing magnetic potential is zero, an important equation that  $I_1W_1=I_2W_2$  is obtained. Hence the measured current  $I_1$  can be determined by  $I_1=I_2W_2/W_1$ . Furthermore the secondary current  $I_2$  can be determined by the current shunt and shown as  $I_2=u_2/R_2$ . As a result, current  $I_1$  can be determined by  $I_1=W_2u_2/W_1R_2$ .

### 2.3 Transfer function of the sensor head $F(s)$

In Figure 1, the sensor head is composed of a toroidal core, AC excitation loop (including AC excitation source and excitation winding), and detection loop (made of detection winding, terminal resistor  $R_M$ , precondition circuit, differential RMS circuit for acquiring the differential RMS of the terminal voltage from the detection winding). The transfer function of the sensor head,  $F(s)$ , can be defined as

$$F(s) = \frac{U_{MdiffRMS}(s)}{I_1W_1(s)} \quad (25)$$

where  $U_{MdiffRMS}(s)$  and  $I_1W_1(s)$  are Laplace transformations of differential RMS  $U_{MdiffRMS}$  and primary ampere-turn  $I_1W_1$ .

A direct quantitative analysis of the transfer function  $F(s)$  is rather involved according to the Laplace transformations of equations (24) and (25) whose Laplace transformations are very complex. This complicated transfer function  $F(s)$  can be represented graphically. And the practical method of obtaining the transfer function  $F(s)$  is generalized as follows:

At first, let the feedback loop is in open circuit and the core is stimulated both by DC and AC source. DC biasing ampere-turn,  $I_1W_1/A$ , denotes abscissa  $x$ -axis, i.e.  $x=I_1W_1$ . Differential RMS values of the terminal voltage of the detection winding,  $U_{MdiffRMS}/V$ , denotes vertical  $y$ -axis, i.e.  $y=U_{MdiffRMS}$ . The plot of  $I_1W_1/A$  as a function of  $U_{MdiffRMS}/V$  is defined as the output characteristic graph of  $I_1W_1$  versus  $U_{MdiffRMS}$  of the sensor head of the proposed DC comparator. This is written symbolically as  $U_{MdiffRMS}=f(I_1W_1)$  or  $y=f(x)$ .

Secondly, we will acquire the experimental data both of  $I_1W_1/A$  and  $U_{MdiffRMS}/V$  and plot the characteristic curve of  $I_1W_1/A$  vs.  $U_{MdiffRMS}/V$ . Some parameters of the prototype comparator are presented in Table 1, where  $D$ ,  $d$  and  $h_D$  are the outside diameter, inside diameter and thickness of the toroidal core stacked by Permalloy 80 iron rings. And the characteristic curve of  $U_{MdiffRMS}/V$  vs.  $I_1W_1/A$  can be acquired and plotted in Fig.3.

**Table 1** Simulation and experimental parameters of the comparator

$L_1=L_2$	3mH	$U_{Sm}$	19.7V
$W_1$	2 Turns	$f$	130.8Hz
$W_S$	100 Turns	$R_S$	135 $\Omega$
$W_M$	390 Turns	$R_M$	10k $\Omega$
$W_2$	400 Turns	$B_S$	0.78 T
$R_1$	300 $\Omega$	$R_2$	100 $\Omega$
$K_p$	3	$T_1$	4.7ms
$h_D$	20mm	$K_D$	undetermined
$D$	150mm	$d$	110mm
Initial permeability	>80000(Gs/Oe)	Curie Tem.	400 $^{\circ}C$
Max. Permeability	600,000(Gs/Oe)	Coercive force	<1(A/m)

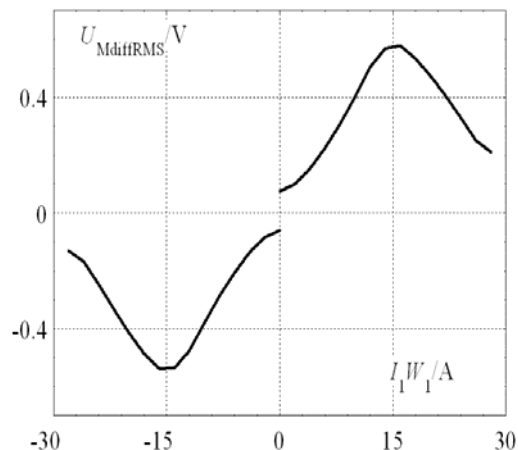


**Fig.3** Experimental relation curve:  $U_{MdiffRMS}/V$  vs.  $I_1W_1/A$

Thirdly, guess the maximum fitting error  $\xi_{max}$  is less than a given tolerance value  $T_E$  (e.g.  $T_E=10^{-5}$ ). Resorting to a least square estimator, we can fit the characteristic curve function, i.e.

$\hat{U}_{MdiffRMS} = \hat{y} = f(I_1W_1) = f(\hat{x})$ . When primary ampere-turns  $I_1W_1 > 0$  (i.e.  $I_1$  is positive current), the fitting polynomial is expressed as follows:

$$\hat{y} = 1.2 \times 10^{-5} x^4 - 7.1 \times 10^{-4} x^3 + 1.2 \times 10^{-2} x^2 \dots - 2.5 \times 10^{-2} x + 8.9 \times 10^{-3} \quad (26)$$

When primary ampere-turns  $I_1W_1 < 0$  (i.e.  $I_1$  is negative current), the fitting polynomial is expressed as follows:

$$\hat{y} = -1.26 \times 10^{-5} x^4 - 7.5 \times 10^{-4} x^3 \dots - 1.2 \times 10^{-2} x^2 - 2.7 \times 10^{-2} x - 7.5 \times 10^{-2} \quad (27)$$

Fig.3 plots the characteristic that  $U_{MdiffRMS}$  varies with the bias number-turns  $I_1W_1$  when CSR is stimulated both by AC voltage source and direct current. Analysis of Fig.4 indicates  $U_{MdiffRMS}$  varies increasingly at first and then varies decreasingly with increasing number-turns  $I_1W_1$ . When the CSR core is in deeply saturation situation,  $U_{MdiffRMS}$  is very small but isn't zero. By varying  $U_{MdiffRMS}$  only

a few tenths of a volt will shows the bias number-turns  $I_1W_1$  isn't zero, i.e.,  $I_1W_1$  is either very small or very large. On the basis of these data plotted in Fig.4 it can be concluded that the output characteristic graph of the sensor head has no false-balance points, which guarantees the stability and reliability of the close-loop operation of the proposed comparator. A comparison of the output characteristic graph of MMC with the proposed comparator indicates that the latter can overcome the problem of the instability of the close-loop control operation.

When current  $I_1$  is positive, the transfer function of the sensor head,  $F(s)$ , can be shown as

$$F(s) = \frac{U_{MdiffRMS}(s)}{I_1W_1(s)} = \frac{2.9 \times 10^{-4}}{s^5} - \frac{4.3 \times 10^{-3}}{s^4} + \dots$$

$$\frac{2.4 \times 10^{-2}}{s^3} - \frac{2.5 \times 10^{-2}}{s^2} + \frac{8.9 \times 10^{-2}}{s}$$

(28)

When current  $I_1$  is negative, the transfer function of the sensor head,  $F(s)$ , can be shown as

$$F(s) = \frac{U_{MdiffRMS}(s)}{I_1W_1(s)} = \frac{-3 \times 10^{-4}}{s^5} - \frac{4.5 \times 10^{-3}}{s^4} \dots$$

$$\frac{2.4 \times 10^{-2}}{s^3} - \frac{2.7 \times 10^{-2}}{s^2} - \frac{7.5 \times 10^{-2}}{s}$$

(29)

#### 2.4 Transfer function analysis of the comparator system

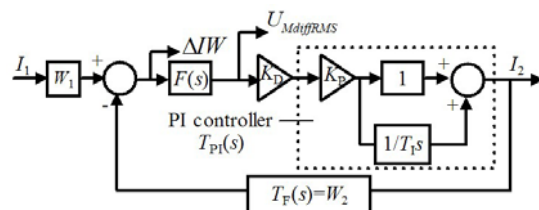


**Fig.4** Control block diagram of the hybrid DC comparator

The main components of the hybrid comparator consists of sensor head  $F(s)$ , power amplifier  $K_D$ , PI controller  $T_{PI}(s)$  and feedback winding  $T_F(s)$ . The control diagram of the presented comparator is shown in Fig.4, where  $\Delta IW$  is the net number-turns and defined as  $\Delta IW = I_1W_1 - I_2W_2$ . Power amplifier will amplify the nonzero deviation voltage  $U_{MdiffRMS}$  that reflects the net number-turns  $\Delta IW$ . Then the deviation voltage  $U_{MdiffRMS}$  (i.e.  $U_{MdiffRMS} \neq 0$ ) is regulated by PI controller and follows into the feedback winding forming a reverse biasing magnetic potential relative to the primary one. Simultaneously the total biasing magnetic potential in core decreases. Hence the deviation voltage  $U_{MdiffRMS}$  decreases. Once the biasing magnetic potential is balanced, the deviation voltage  $U_{MdiffRMS}$  does not exists and the zero-flux state is gained, i.e.  $\Delta IW = I_1W_1 - I_2W_2$ . Thus, an important equation that  $I_1W_1 = I_2W_2$  can also be obtained from the homeostasis of the comparator. The comparator can readily perform the DC measurement operation.

Transfer function of the PI controller  $T_{PI}(s)$  and feedback winding  $T_F(s)$  are respectively expressed as

$$T_{PI}(s) = K_p(1 + 1/T_i s) \quad (30)$$

$$T_F(s) = W_2 \quad (31)$$

where  $K_p$  is proportion factor,  $T_i$  is integration time, see Table 1. The transfer function of the whole comparator sensor system,  $T(s)$ , can be deduced as follows:

$$T(s) = \frac{I_2}{I_1} = W_1 \frac{F(s)K_D K_p(1 + T_i s)}{T_i s + W_2 F(s)K_D K_p(1 + T_i s)}$$

(32)

where  $K_D$  stands for power amplifier parameter and is undetermined variable.

$$1 < K_D \ll \frac{0.1}{W_2 K_p} \approx 6.3 \times 10^5 \quad (35)$$

2.5 Stability analysis of the DC comparator

The characteristic equation of  $T(s)$  can be expressed as

$$P(s) = T_1 s + W_2 F(s) K_D K_p (1 + T_1 s) \quad (33)$$

The stability of the whole measurement sensor system is of great importance to the normal operation for the comparator. To satisfy the measuring requests, some considerations of the static error and dynamic characteristic of the comparator sensor system must be emphasized. Eqn. (32) indicates that the whole comparator belongs to a high-order system. The stability can conveniently be judged and controlled by the Routh criterion. Of the three parameters  $K_D$ ,  $K_p$ ,  $T_1$ , only parameter  $K_D$ , the power amplifier multiple is unknown and functions for regulating the stability of the comparator system. Hence, other two parameters can be disposed of rather quickly. Assuming characteristic equation is zero and shown by

$$P(s) = T_1 s + W_2 F(s) K_D K_p (1 + T_1 s) = 0 \quad (34)$$

The necessary and sufficient precondition of the stability of the measuring system is that all of the real parts of the characteristic roots of  $P(s)$  are negative. It is necessary for us to solve the characteristic equation for  $K_D$ . In our discussion of dynamic property of the whole comparator, we shall restrict our attention to the positive case ( $I_1 > 0$ ). Analyzing method for the negative case ( $I_1 < 0$ ) is the same to the positive and omitted in the paper. As a result, substituting known parameters  $K_p$ ,  $T_1$ , and Eqn. (32) into the characteristic Eqn. (34),  $K_D$  may be limited by

Thus, the unit-step response of the comparator sensor system can be deduced as follows:

$$I_2 = T(s) \frac{1}{s} = W_1 \frac{F(s) K_D K_p (1 + T_1 s)}{T_1 s^2 + W_2 F(s) K_D K_p (1 + T_1 s)s} \quad (36)$$

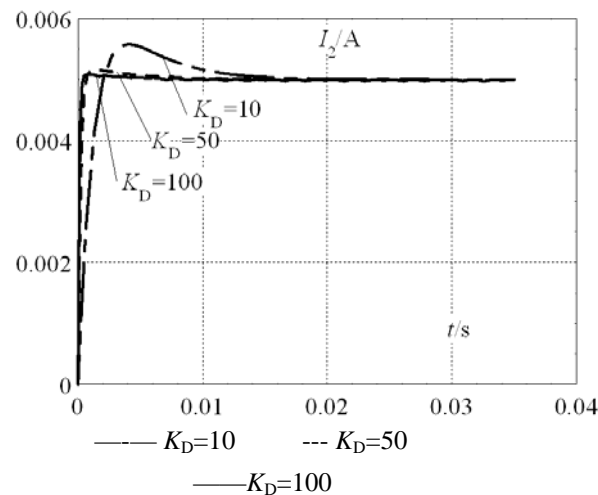


Fig.5 Unit-step response of the hybrid self-balancing DC comparator

The dynamic properties of the comparator are so important that such dynamic qualification indexes centered on the Eqn. (35) as overshoot (less than 50%), rise time, stable time and governing time, must be taken into account. thus, parameter  $K_D$  must be limited by

$$K_D \leq 1000 \quad (37)$$

Based on the simulation tools of the MATLAB SIMULINK environment (see [10]), the unit-step response with the changes of the parameter  $K_D$  of the hybrid comparator is plotted in Fig.5. Analysis of Fig.5 shows the overshoot and stable time will increase obviously with  $K_D$  enhancement. Thus, parameter  $K_D$  must be properly selected for the comprehensive considerations of the stability,

overshoot, rise time, stable time and governing time of the comparator system.

### 2.6 Static error analysis of the whole DC comparator

The amplifier multiple of the open-loop of the comparator,  $K_{OP}$ , is defined as the products of each component's amplifier multiple and shown as follows:

$$K_{OP} = 8.9 \times 10^{-2} \times W_1 \times W_2 \times K_D \times K_P \quad (38)$$

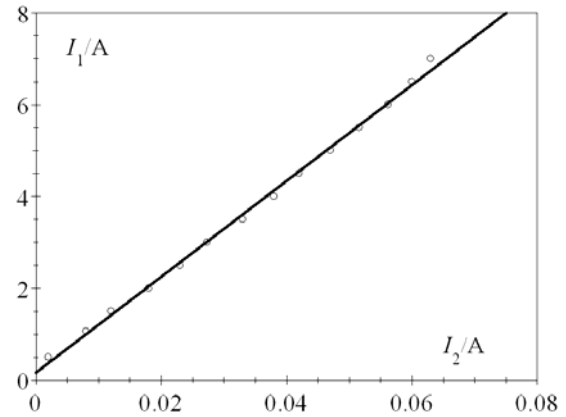
And the static error of the comparator is determined as

$$\sigma_s = 1/K_{OP} \quad (39)$$

The foregoing provides a basis for this proposed comparator, although it cannot be considered as a precise proof.

## 3. Experimental results

The CSR core is a toroidal core stacked by Permalloy 80 iron rings. Permalloy 80 is an ideal material for CSR applications. Squariness coefficient is almost as high as the cobalt based amorphous material and flux density is higher. Some important parameters of the experimental prototype comparator based on Fig.1 are listed in the Table 1. Thus, in the above prototype comparator analysis,  $K_D = 100$ .



○ Experimental points — Fitting curve  
**Fig.6** Experimental results of the proposed self-balancing DC comparator

The experimental points are plotted and joined, thus forming the curve represents the sensor function for the comparator and illustrates as Fig.6, where vertical y-axis stands for the measured current  $I_1/A$ , and abscissa x-axis denotes the secondary current  $I_2/A$ . The characteristic graph of  $I_1$  against  $I_2$  can be determined by

$$I_1 = K_S I_2 + K_{DB} \quad (40)$$

where  $K_{DB}$  is offset value of the comparator.  $K_S$  is the ratio of measured current  $I_1/A$  to the secondary current  $I_2/A$  and also is called the ratio of the output static curve of the proposed comparator and expressed as

$$K_S = I_1/I_2 \quad (41)$$

Since the output static curve of the comparator is linear, the sensitivity of the comparator is equal to the slope ratio of the experimental curve, and determined by

$$S_I = K_S = W_2 G / W_1 \quad (42)$$

where  $G$  is the total gain of the feedback loop (usually  $G \neq 1$ ). The experimental value  $K_S$ ,  $S_I$  and  $K_{DB}$  are listed as follows:

$K_S=S_I=104$ ,  $K_{DB} =0.02A$ . And the linearity correlation coefficient of the fitting curve of Fig.6 based on the experimental data is 0.999.

For counteracting the offset value of the comparator, some compensation measures are necessary (i.e. the secondary compensation measures are usually adopted). Some details of the secondary compensation measures of the comparator are omitted in the paper.

#### 4. Conclusions

With the inclusions of detection winding and secondary winding for the conventional CSR configuration, things are different. The proposed comparator just is centered on the above construction of the CSR. The detection-winding functions as an indicator that reflects the DC biasing magnetic potential. The secondary winding acts as a compensation one. The reduction of the comparator eliminates unnecessary core and complicate peripheral circuit, thereby saving cost, space and weight. And the comparator has the characteristic of four windings wound around the toroidal core and simple peripheral circuits. The comparator is usually operated by the counterbalance of an ascending and a descending DC number-turn. The differential RMS of half waves of the terminal voltage from the detection winding is verified to fit for the feedback variance for the hybrid comparator. And the output characteristic curve of the sensor has no false points, which guarantees the stability and reliability of the close-loop control operation of the comparator. The analysis method of the transfer function of the sensor head resorting to the curve fitting technique is useful to determine and optimize

the dynamic property of the comparator.

#### 5. References

- [1] A. Barili, A. Brambilla, G. Cottafava, et al. "A simulation model for the saturable reactor", IEEE Transactions on Industrial Electronics, vol: 35, no: 2, pp.301-306, May 1988.
- [2] M. MacMartin, N. Kusters. "A self-balancing direct current comparator for 20 000 amperes", IEEE Transactions on Magnetics, vol: 1, no: 4, pp. 396-402, Dec 1965.
- [3] Li Weibo, Mao Chengxiong, Lu Jiming. "Study of the Virtual Instrumentation Applied to Measure Pulsed Heavy Currents", IEEE Transactions on Instrumentation & Measurement, 2005, 54(1): 284-288.
- [4] Mingjun Zhu, Xu, Ken, "A calibrating device for large direct current instruments up to 320 kiloampere-turns", IEEE Transactions on Instrumentation & Measurement, vol: 47 (3), pp. 711-714, June 1998.
- [5] K. Harada, Y. Ishihara, T. Todaka. "A novel high power factor converter using a magnetic amplifier", IEEE Transactions on Magnetics, vol: 32, no: 5, pp. 5013 – 5015, Sept. 1996.
- [6] E. So. "The application of the current-comparator technique in instrumentation and measurement equipment for the calibration of non-conventional instrument transformers with non-standard rated outputs", IEEE Transactions on Power Delivery, vol: 7, no: 1, pp. 46-52, 1992.
- [7] Li Weibo, Mao Chengxiong, Lu Jiming. A novel fiber-optic current measurement instrument for high-power laser source. Journal of Electrical and Electronics

- Engineering, vol: 3, no: 2, pp.835-841, 2003.
- [8] Li Weibo, Mao Chengxiong, Lu Jiming. Some considerations of designing a high performance Rogowski coil for pulsed current measurement, Journal of Electrical and Electronics Engineering, vol: 7, no: 1, pp.7-12, 2006.

### **Biographies**

Li Weibo received his B.S. degrees in mechanical engineering from Sichuan University of Science & Technology (SUCT), Chengdu, in 1997. And he received his M.S. degrees and P.H. degrees in Department of Electrical Engineering from Huazhong University of Science & Technology (HUST), Wuhan, respectively in 2001 and 2006. He is currently in the Naval Engineering University. He is a member of IEEE. Now he focuses all his attention on measurement and control technologies.